Thermodynamic Control on Biogeography and Functioning of Rare-Biosphere Propionate Syntrophs in Paddy Field Soils

Yidan Jin
Peking University https://orcid.org/0000-0001-7600-1032
Shuo Jiao
Northwest Agriculture and Forestry University
Yahai Lu (luyh@pku.edu.cn)
Peking University

Research

Keywords: Rare biosphere, Propionate syntrophs, Biogeography, Methanogenesis, Paddy soil

Posted Date: May 1st, 2020

DOI: https://doi.org/10.21203/rs.3.rs-23525/v1

Abstract

Background

Global biogeochemical processes are not only gauged by dominant taxa of soil microbiome but also depend on the critical functions of “rare biosphere” members. Here we evaluated the biogeographical pattern of “rare biosphere” propionate-oxidizing syntrophs in 113 paddy soil samples collected across eastern China.

Results

The relative abundance, functioning capacity and growth potential of propionate-oxidizing syntrophs were analyzed to provide a panoramic view of syntroph biogeographical distribution at the continental scale. The relative abundances of four syntroph genera, *Syntrophobacter*, *Pelotomaculum*, *Smithella* and *Syntrophomonas* were significantly greater at the warm low latitudes than at the cool high latitudes. Correspondingly, the functioning potential of propionate degradation was greater in the low latitude soils compared with the high latitude soils. The slow rate of propionate degradation in high latitude soils resulted in a greater fold change in increase of the relative abundance, probably due to the growth rate-yield tradeoff relationship. The mean annual temperature (MAT) is the most important factor shaping the biogeographical pattern of propionate-oxidizing syntrophs, with the next factor to be the total S content (TS) in soil.

Conclusions

We suggest that the effect of MAT is related to the Gibbs free energy change, in which the endergonic tension of propionate oxidation is leveraged with the increase of MAT. The TS effect is likely due to that some propionate syntrophs can facultatively perform sulfate respiration.

Background

Soil microbiome plays the vital role in regulating global biogeochemistry. It has been recently documented that albeit immense biodiversity of soil microbiome, only a few hundreds of phylotypes are prevalent across global soils and these dominant phylotypes display distinct biogeographical distribution according to their habitat preferences [1]. The factors shaping the biogeographic patterns of global soil microbiome include climatic factors, edaphic properties and biological interactions [2–6]. Identification of soil dominant taxa, their geographical distributions and the controlling factors provide a “most-wanted” list for cultivation and genomic scrutiny that shall help decoding biogeochemical mechanisms and pave a way toward developing global Earth system models that are soil context-dependent [1, 7, 8]. The dominants-hunting approaches, however, will inevitably overlook the function of “rare biosphere” specialists [9]. It has been understood that biogeochemical processes are not only gauged by dominant

taxa that operate through biomass turnover but also depend on critical functions of specialist members [7]. A typical example is microbial syntrophs, which plays a critical role in anaerobic decomposition of organic matter and methanogenesis but have only low relative abundance in natural environments like paddy field soils [10, 11].

Complex organic matter in anoxic environments is degraded by an anaerobic food chain comprising primary and secondary fermentors, homoacetogens and methanogens [12, 13]. A series of short-chain fatty acids and alcohols (SCFAs) are transiently accumulated as intermediate products during the process [12, 14–16]. Syntrophic cooperation between secondary fermentors (i.e. the syntrophs) and methanogens is essential to degrade these chemicals, which otherwise cannot be broken down by either guilds alone [13, 17, 18]. Propionic acid is one of major intermediates accounting for up to 30% of the total CH_4 formation in paddy soils [14, 19]. The process of propionate degradation is thermodynamically the most unfavorable among common SCFAs like ethanol and butyrate, making propionate degraders being the slowest in growth and sensitive to environmental conditions [17, 20, 21]. Identifying propionate-oxidizing key taxa and delineating their biogeographical distribution are therefore important for better understanding and predicting organic matter decomposition and C cycling in anoxic environments including natural wetlands and paddy field soils.

Paddy field soils are human-managed ecosystems and an important contributor to global CH_4 emissions [22, 23]. About 90% of paddy fields are located in Asia with 20% of that in China [24]. Rice production in China is dominated by irrigated systems, which is mainly distributed in the lowland of eastern China, extending from warm sub-tropics at 18°N latitude to cool temperate regions at 50°N [25]. The long history of rice cultivation makes the region an ideal site for microbial biogeography investigation that is independent of large scale variations of vegetation and soil. In the present study, we collected 113 paddy field soils from different regions across eastern China with a latitudinal distance of 3 689 kilometers. The potentials of propionate degradation in each soil were determined through anaerobic incubations in laboratory. The composition and abundance of propionate syntrophs in original soils and soil samples after anaerobic incubations were investigated using high throughput sequencing of bacterial 16S rRNA genes. We show here that temperature and the total S content in soil are the most important factors shaping the biogeographic distribution and functioning of propionate-oxidizing syntrophs in paddy field soils at the continental scale.

Methods

Soil sampling and analysis of basic soil properties

One hundred thirteen soil samples were collected from paddy fields across eastern China in the summer from July to September of 2017. At each site, five soil sub-samples were taken at a depth of 0–15 cm and mixed thoroughly. The collected paddy soils were placed in ziplock plastic bags and transported to lab at 4 °C within 36 h. Standard soil testing procedures were followed to measure soil pH, cation exchange capacity (CEC), organic matter (OM), dissolved organic carbon (DOC), total nitrogen (TN), total

phosphorus (TP), total sulfur (TS), total Fe (TFe) and fourteen additional properties [26]. Climatic variables, including mean annual temperature (MAT) and mean annual precipitation (MAP) at each sampling site were obtained using site coordinates from the WorldClim database (www.worldclim.org).

Soil slurry preparation and anaerobic incubation

To determine the potentials of propionate degradation, soil samples were subjected to anaerobic incubation under laboratory conditions with propionate as a sole substrate. Soil samples were suspended in autoclaved degassed water at a soil-to-water ratio of 1:5 (1 g dry weight soil plus 5 ml autoclaved degassed water). Aliquots (45 ml) of homogenized soil slurry were transferred into 120 ml sterile serum bottles which were capped with black butyl rubber stoppers and aluminum crimps. The sodium propionate was added into the bottles to a final concentration of 10 mM. The bottles were vigorously shaken by hand to homogenize soil slurries, flushed with N_2 for 5 min and then incubated under the dark at 30 °C without shaking. Experiment was carried out in triplicate.

Chemical analyses

The gaseous samples (200 μL) were regularly collected from the headspace of incubation bottles using pressure-lock analytical syringe (Baton Rouge, LA). The CH_4 concentration was analyzed by Agilent 7890B gas chromatograph (Agilent Technologies, USA) equipped with flame ionization detector (FID) and thermal conductivity detector (TCD) [27]. For the analysis of fatty acids, 0.8 ml of liquid samples were collected from the bottles with sterile syringes and centrifuged for 10 min at 6870 *g* at 4 °C. The supernatants were filtered through 0.22 μm cellulose membrane filters and acidified by 18.4 mM H_2SO_4. Acetate, propionate and butyrate were analyzed by HPLC (Agilent 1260, USA) equipped with Zorbax SB-AQ C18 column and UV detector at 210 nm [28].

Soil DNA extraction and Illumina sequencing of 16 S rRNA genes

Microbial DNA samples were extracted both from original soil samples and from soil samples after anaerobic incubations. For the original soil samples, 0.5 g of fresh sample was used for DNA extraction using the FastDNA SPIN Kit (MP Biomedicals, USA) according to the manufacturer's protocol [26]. For the soil samples after anaerobic incubations, 2 ml of soil slurries were collected at the time when at least 90% of propionate was consumed in each soil incubation. The date of sampling differed among soil samples because the time for propionate consumption varied markedly. The collected soil slurries were transferred to the sterile centrifugal tube and centrifuged for 10 min at 6 870 *g* at 4 °C. Total genomic DNA was extracted from the precipitated samples using the FastDNA SPIN Kit. DNA samples extracted in triplicate for each soil sample were pooled in equal-volume and then used for high-throughput sequencing on an Illumina Miseq platform [29-31]. Primer set Ba338F (5'-ACTCCTACGGGAGGCAGCAG-3') and 806R (5'-GGACTACHVGGGTWTCTAAT-3') was employed to amplify V3-V4 regions of the bacterial 16S rRNA genes. Sequences were split into groups according to taxonomy and assigned to operational taxonomy units (OTUs) at a 3% dissimilarity level using the UPARSE pipeline [32]. OTUs with fewer than

two sequences were removed, and representative sequence of each OTU was assigned to a taxonomic lineage by RDP classifier against the SILVA database.

Statistical analyses

To correct for sampling effort in DNA sequencing (number of analyzed sequences per sample), the sequence number was rarefied at 27 812 high-quality sequences per sample for the original soil samples and 18 441 high-quality sequences per sample for the samples after anaerobic incubations, respectively [26]. Bacterial α-diversity (Shannon index) was calculated using QIIME (http://qiime.org/index.html). Bacterial β-diversity was estimated according to the Bray-Curtis distance between samples. Metacommunity co-occurrence network analysis at OTU or genus levels was based on Pearson's correlation coefficient between microbial taxa and visualized by Gephi 0.9.2 [33]. The circle phylogenetic tree was built with FastTree using a GTR model and visualized by iTOL after the sequence cutoff and gap trimming treatment by Silva Incremental Aligner (SINA v1.2.11) and trimAl, respectively [34, 35]. The phylogenetic trees were constructed using the neighbor-joining algorithm with 1 000 Bootstrap replications in MEGA 7.0.14.

To build predictive maps of the spatial distributions of the bacterial syntroph taxa, we used a Kriging interpolation method with the "automap" package in R to estimate the relative abundance and the changes of syntrophs in paddy soils. Kriging interpolations were performed with the best-fitted variogram model through cross validation, which was performed using autoKrige.cv in the "automap" package by setting the parameter "nfold" to 113, the number of soil samples in analysis [36]. The correlation between estimated values of sampling site in cross validation and the observed values at the corresponding sites were displayed with the Pearson correlation coefficient and *P* value in the map. The predictive maps were also build for the functional potential of propionate degradation, which was evaluated based on the time lapse for CH_4 production from propionate oxidation and the maximum rate of methanogenesis during anaerobic incubation and for the Gibbs free-energy changes ($\triangle G^{0'}$) of propionate oxidation, which were calculated by setting standard conditions except temperature.

Regression and correlation analyses were used to delineate the relationship between environmental factors, syntroph abundances and functional potentials. Boruta algorithm implemented in R package "boruta" was used to identify the relevant environmental factors and estimate their importances to the relative abundance of propionate syntrophs in paddy soils [37].

The processing and visualization of all data were conducted in the R environment (v3.6.0; http://www.r-project.org/) using the following packages unless otherwise indicated: ggplot2 [38], Boruta [37], corrplot [39], automap [40], pheatmap [41] and psych [42].

Results

Biogeographical distribution of propionate syntrophs

A total of 6 204 541 high quality sequences of bacterial 16S rRNA genes were obtained from 113 paddy soil samples, which are clustered into 27 411 OTUs. The most dominant OTUs were affiliated to *Proteobacteria*, *Firmicutes*, *Actinobacteria*, *Chloroflexi*, *Acidobacteria*, *Nitrospirae* and *Gemmatimonadetes* (Additional file 1: Supplementary Figure 1). OTUs that were assigned to four genera of propionate-oxidizing syntrophs (i.e. *Syntrophobacter*, *Pelotomaculum*, *Smithella* and *Desulfotomaculum*) and those to *Syntrophomonas* were retrieved for analysis in this study (Additional file 1: Supplementary Figure 2). *Syntrophomonas* are not known to oxidize propionate but butyrate and up to C_{10} fatty acids [43]. The inclusion of *Syntrophomonas* in analysis was due to the fact that *Smithella*, which utilize the C_6 dismutation pathway, can release butyrate as an intermediate product into environment, which is then metabolized by *Syntrophomonas* [44]. A total of 30 OTUs belonging to five syntroph genera were retrieved.

The total abundance of all five syntroph genera together (referred to synTotal) ranged from 0.01 to 0.34% across 113 soil samples. This low abundance certificates that syntrophs in paddy soils belong to a subset of “rare biosphere” community (defined as individual species or OTUs accounting for <0.1% of the total abundance). Albeit “rare” in relative abundance, the synTotal displayed a distinct geographical distribution, showing the highest abundance in the warm low latitude soils and gradually decreasing towards the high latitude regions (Fig. 1A). The conventional geographical division separates China into the south (low latitude) and the north (high latitude) regions according to the Qinling Mountains-Huaihe River Line (latitude ≈ 32°), a critical geographical boundary for climate, landform and soil conditions [45]. Accordingly, we summarized our soil samples into the low latitude and the high latitude groups, respectively. The mean relative abundance of the low latitude group is significantly greater (by 1.84-fold) than that of the high latitude group (bottom-left of Fig. 1A). In line with the synTotal, the α-diversity of syntrophs, estimated based on OTU richness, significantly decreased with the increase of latitude (Fig. 1B). We then identified the key environmental factors related to the synTotal distribution through Spearman correlation analysis. MAT and TS (total soil S) were identified as the two most important factors followed by NH_4^+-N, soil OM, MBC and TN (Fig. 1C). Soil CEC and pH showed the negative correlations. The importance index estimated based on Boruta algorithm reiterated that MAT and TS were the two most important factors linking to biogeographical distribution of synTotal (Fig. 1C).

To compare the distribution of different syntrophs, the relative abundances of five syntroph genera were individually analyzed (Additional file 1: Supplementary Figure 3). The distributions of *Syntrophobacter*, *Pelotomaculum*, *Smithella* and *Syntrophomonas* were in consistence with that of the synTotal (Additional file 1: Supplementary Figure 3A-D). *Desulfotomaculum* was an exception showing the highest abundance in the middle latitude regions (Additional file 1: Supplementary Figure 3E). Division of the low and high latitude groups revealed that the mean relative abundances of *Syntrophobacter*, *Syntrophomonas* and *Pelotomaculum* were significantly greater in the low latitude regions (Additional file 1: Supplementary Figure 3F), in consistence with the synTotal. *Syntrophobacter* showed the greatest mean relative abundance followed by *Syntrophomonas* and *Smithella*, while *Pelotomaculum* and *Desulfotomaculum* showed very low abundances (Additional file 1: Supplementary Figure 3F).

Biogeographical feature of syntroph functioning potentials

Next we evaluated the biogeographical feature of syntroph functioning potentials. For this purpose, fresh soil samples were incubated under anaerobic conditions with addition of 10 mM propionate. We observed the CH_4 production until >90% of the added propionate consumed. Three distinct patterns of methanogenesis were identified according to the time lapse required for CH_4 production from propionate oxidation (Fig. 2). The pattern I comprised 45 soil samples with the time lapse of 13 d to 27 d, representing the fast rate group of syntrophic metabolisms (Fig. 2A). A greater proportion of soil samples tends to be located at the low latitudes in this group. The pattern II, including 51 samples, represented the median rate of syntrophic metabolisms (28 d to 43 d), which did not show a distinct latitudinal tendency (Fig. 2B). The pattern III comprising 17 soil samples required 44 d to 82 d for CH_4 production from propionate oxidation and hence represented the slow rate group. The soils of this group were distributed mainly in the cool high latitude regions (Fig. 2C). The analyses of propionate consumption confirmed the separation of soil samples into three groups (Fig. 3A). Acetate was a major intermediate detected in all samples (Fig. 3B). Butyrate was detected in 28.3% of soil samples (detection limit of 0.05 mM) (Fig. 3C), with the highest concentration occurring in the pattern III soils (Fig. 3C). Taking all soil samples together, the time lapse for methanogenesis from propionate degradation displays an explicit biogeographical pattern, being significantly slower in the high latitude soils than in the low latitude soils (Fig. 4A). The linear least squares regression revealed that the time lapse for methanogenesis was significantly negatively correlated with the relative abundance of synTotal in original soils, MAT, TS, and other edaphic factors including soil OM, MBC, available Fe, Cu and Mn (Fig. 4C). The functional potential of propionate degradation can also be inferred from the maximum rate of methanogenesis (Fig. 4B), which supports the biogeographical tendency revealed by the time lapse (i.e. the shorter the time lapse, the greater the maximum rate).

Shift of microbial community during the anaerobic incubation

At the end of anaerobic incubations, the structure of microbial community in soil samples was revisited. The community composition at the phylum level did not show significant changes between original soil samples and those after anaerobic incubations. The relative abundances of a few phyla, however, changed markedly (Additional file 1: Supplementary Figure 4A). Specifically, the relative abundances of *Proteobacteria* and *Acidobacteria* decreased over the incubations while those of *Actinobacteria*, *Firmicutes* and *Chloroflexi* increased. Notably, the α-diversity of bacterial communities at the OTU level showed a substantial decline at the end of incubation compared with original soils (Additional file 1: Supplementary Figure 4B). The β-diversity at the genera level showed the separation of soil samples into two clusters for the low latitude and high latitude soils, respectively (Additional file 1: Supplementary Figure 4C). The co-occurrence network analysis of the top 10% OTUs confirmed that the OTUs for the low and high latitude regions tended to group separately (Additional file 1: Supplementary Figure 4D). These results indicate that the bacterial community shifted significantly during anaerobic incubation, while the separation of metacommunities into the low latitude and the high latitude groups remained robust.

The relative abundance of syntrophs except *Desulfotomaculum* increased markedly after the incubation with the maximum abundance of synTotal reaching to 12.5%, indicating significant growth. We estimated the increase of individual syntrophs by calculating the logarithmic (log_2) fold change (R) of the relative abundance over the incubation. The relative abundance of *Desulfotomaculum*, which was low at the beginning, did not change over the incubation, indicating no response to propionate. Other four genera showed significant increases but to different extents (Fig. 5). *Pelotomaculum* showed the greatest increase, followed by *Smithella* and *Syntrophomonas*, while *Syntrophobacter* exhibited the least increase (Fig. 5F). Strikingly, the relative increases of syntrophs showed an opposite geographic tendency compared with their abundances in original soils (Fig. 2). The log_2 R values for *Syntrophobacter*, *Syntrophomonas* and *Smithella* increased with the increase of latitude (Fig. 5A,B,D). The values for *Pelotomaculum* also increased with latitude, though showing the highest value at the middle latitude (Fig. 5C). These results indicate that propionate syntrophs in anaerobic incubation grew to a greater extend in soil samples from the high latitudes than those from the low latitudes.

Discussion

Given their low abundance in paddy soils *in situ* but playing the critical role in oxidizing intermediate products during anaerobic decomposition of organic matter, propionate-oxidizing syntrophs represent the typical example of rare but important taxa of soil microbiome. Here we show that the relative abundance of propionate syntrophs is significantly correlated with MAT (Fig. 1). Based on the time lapse for methanogenesis from propionate oxidation, we further reveal that the biogeographical pattern of syntroph functioning potentials (Figs. 2,3) is in accordance with their relative abundances in soils. It has been documented that within the physiological range, the microbial diversity, metabolic activity and population growth rates in terrestrial ecosystems increase exponentially with temperature [46]. Hence, climate warming is expected to accelerate temporal turnover and divergent succession of microbial communities in soils [47, 48]. However, such a temperature impact can be universal to all microbes. Syntrophs are known to have a specific lifestyle by living at thermodynamic limit. In order to obtain a deeper insight into temperature effect, we calculated the standard Gibbs free-energy changes ($\triangle G^{0'}$) for the reaction of propionate oxidation [$CH_3CH_2COO^-(aq) + 2H_2O(l) — CH_3COO^-(aq) + 3H_2(g) + CO_2(g)$] (Fig. 6A). Temperature was assumed to be an only variable with other variables set to standard conditions and the $\triangle G^{0'}$ was calculated as described [49]. The values of $\triangle G^{0'}$ (in positive) increased with the increase of latitude. The linear least squares regression revealed that the values of $\triangle G^{0'}$ are significantly negatively correlated with the relative abundance of synTotal and the maximum rate of CH_4 production and positively with the time lapse for methanogenesis from propionate degradation (Fig. 6B-D). These correlations suggest that the decrease of free energy changes (in positive values) in the south China alleviates the thermodynamic tension, hence supporting the greater abundance of syntrophs and the faster rate of propionate oxidation compared with those in the north China.

We found that the total S in soil was the second important factor. This was possibly due to the fact that many of propionate syntrophs like *Syntrophobacter fumaroxidans* and *Pelotomaculum*

thermopropionicum are facultative sulfate reducers [50–52]. In the presence of sulfate these organisms tend to perform anaerobic sulfate respiration instead of syntrophy with methanogens for maximizing energy conservation [52–56]. Notably, while the relative abundances of *Syntrophobacter*, *Smithella* and *Syntrophomonas* in paddy soils were significantly correlated with TS, that of *Pelotomaculum* did not (Fig. 1C). Therefore, individual syntrophs have different responses to TS. Besides TS, the relative abundances of syntrophs were also positively correlated with the contents of soil OM, total N, MBC, and in addition the functioning potential was correlated with the contents of trace elements Fe, Cu and Mn (Fig. 4C). Since a high soil OM content is usually associated with high TN, MBC and trace element contents and even TS, these edaphic factors are possibly co-variables, and the positive correlations possibly indicate the favorable living conditions for most microbes including syntrophs.

Anaerobic incubation caused a marked shift of soil bacterial community (Additional file 1: Supplementary Fig. 4). Specifically, the relative abundances of syntrophic populations increased by up to 284-fold over the incubation. The increase in relative abundances, however, differs among five syntroph genera. *Pelotomaculum* showed the greatest growth, followed by *Smithella* and *Syntrophomonas* while that of *Syntrophobacter* and *Desulfotomaculum* being the least (Fig. 5). These results indicate that *Pelotomaculum* species are the most important syntrophs metabolizing propionate in paddy soils across a wide geographical location. *Smithella* in combination with *Syntrophomonas* are the next important group, while *Syntrophobacter* play only a minor role and that of *Desulfotomaculum* is negligible. *Pelotomaculum* and *Smithella* are known to use the methylmalonyl-CoA (MMC) pathway and the C_6 dismutation route, respectively [20, 44, 57, 58]. *Smithella* are considered to tolerate a stricter thermodynamic condition than the MMC-utilizing syntrophs [59]. In supporting this idea, we found that the maximum growth of *Pelotomaculum* happened at the middle latitudes while that of *Smithella* and *Syntrophomonas* occurred at the further north (Fig. 5).

The increase in relative abundances, expressed as $\log_2 R$, tends to be greater in the high latitude soils relative to the low latitude soils (Fig. 5), in contrast to the geographical distribution of relative abundances in original soils (Fig. 1). Two plausible explanations may cause this result. First, with identical quantity of propionate consumed, a greater fold change in relative abundance could be expected for soils having the lower initial abundances. Second, the anaerobic incubations were stopped when > 90% of propionate were consumed, which made the duration of incubation varying from 13 d to 82 d across different soils (Fig. 2). With identical quantity of substrate consumption, a longer duration would be expected to produce a greater biomass (yield) [60]. Such a rate-yield tradeoff relationship has been demonstrated in *E. coli* [61, 62] and methanogens [63]. It remains, however, unknown if such a relationship also occurs for propionate syntrophs in paddy soils *in situ*.

Conclusions

In the present study, we demonstrate that both the relative abundance and functioning potential of propionate syntrophs in paddy field soils exhibit a distinct biogeographical pattern. MAT and TS are identified to be two most important factors related to the biogeographical distribution. The temperature

effect is very likely related to thermodynamic conditions, which are improved with the elevation of temperature. The effect of soil S content is possibly due to that some facultative propionate syntrophs perform sulfate respiration in the presence of sulfate. Though difference only in 6.7 °C in MAT, the mean time lapse for methanogenesis from propionate degradation was approximately 30 d longer in the high latitude soils relative to the low latitude soils. This result, on the one hand, indicates that the rates of organic matter decomposition and C cycling are substantially lower in the cool high latitude regions. On the other hand, it suggests that the global warming, which is occurring to a greater extent at the high latitudes, can cause a significant acceleration of organic matter decomposition and C cycling in the high latitude soils.

Declarations

Ethics approval and consent to participate

Not applicable

Consent for publication

Not applicable

Availability of data and material

The datasets supporting the conclusions of this article are available in the NCBI Sequence Read Archive under BioProject PRJNA544819 and PRJNA601098 that are publicly accessible at https://www.ncbi.nlm.nih.gov. R codes on the statistical analyses are available at https://github.com/jinyidan/Rare-Biosphere-Propionate-Syntrophs-in-Paddy-Field-Soils.

Competing interests

The authors declare that they have no competing interests.

Funding

This work was made possible through two NSFC (National Natural Science Foundation of China) grants (91951206, 41630857) and a grant from National Basic Research Program of China (2016YFD0200306).

Authors' contributions

Y.L., S.J., Y.J. designed the study. S.J. conducted field soil sampling. Y.J. and S.J. executed lab work. Y.J., S.J. and Y.L. analyzed the data. Y.L. and Y.J. wrote the manuscript. All authors read and approved the final manuscript.

Acknowledgements

Not applicable

Additional File

Additional file 1: **Supplementary Figure 1.** Phylogenetic relationship of 528 dominant OTUs (top 2.5%) retrieved from 113 paddy field soils. **Supplementary Figure 2.** Neighbor-joining tree of 16S rRNA gene sequences related to five syntroph genera including representative sequences retrieved from this study and the reference sequences. **Supplementary Figure 3.** Biogeographical distributions of five syntroph genera in paddy field soils across eastern China. **Supplementary Figure 4.** Shift of bacterial community in paddy soils in response to anaerobic incubation. (PDF 7223 kb)

References

1. Delgado-Baquerizo M, Oliverio AM, Brewer TE, Benavent-Gonzalez A, Eldridge DJ, Bardgett RD, et al. A global atlas of the dominant bacteria found in soil. Science. 2018;359:320–5.
2. Garbeva P, van Veen JA, van Elsas JD. Microbial diversity in soil: selection of microbial populations by plant and soil type and implications for disease suppressiveness. Annu Rev Phytopathol. 2004;42:243–70.
3. Schlatter DC, Bakker MG, Bradeen JM, Kinkel LL. Plant community richness and microbial interactions structure bacterial communities in soil. Ecology. 2015;96:134–42.
4. Bahram M, Hildebrand F, Forslund SK, Anderson JL, Soudzilovskaia NA, Bodegom PM, et al. Structure and function of the global topsoil microbiome. Nature. 2018;560:233–7.
5. Rillig MC, Ryo M, Lehmann A, Aguilar-Trigueros CA, Buchert S, Wulf A, et al. The role of multiple global change factors in driving soil functions and microbial biodiversity. Science. 2019;366:886–90.
6. Steidinger BS, Crowther TW, Liang J, Van Nuland ME, Werner GDA, Reich PB, et al. Climatic controls of decomposition drive the global biogeography of forest-tree symbioses. Nature. 2019;569:404–8.
7. Crowther TW, van den Hoogen J, Wan J, Mayes MA, Keiser AD, Mo L, et al. The global soil community and its influence on biogeochemistry. Science. 2019;365:772.
8. van den Hoogen J, Geisen S, Routh D, Ferris H, Traunspurger W, Wardle DA, et al. Soil nematode abundance and functional group composition at a global scale. Nature. 2019;572:194–8.
9. Lynch MDJ, Neufeld JD. Ecology and exploration of the rare biosphere. Nat Rev Microbiol. 2015;13:217–29.
10. Lueders T, Pommerenke B, Friedrich MW. Stable-isotope probing of microorganisms thriving at thermodynamic limits: syntrophic propionate oxidation in flooded soil. Appl Environ Microbiol. 2004;70:5778–86.
11. Gan Y, Qiu Q, Liu P, Rui J, Lu Y. Syntrophic oxidation of propionate in rice field soil at 15 and 30 °C under methanogenic conditions. Appl Environ Microbiol. 2012;78:4923–32.
12. Glissmann K, Weber S, Conrad R. Localization of processes involved in methanogenic in degradation of rice straw in anoxic paddy soil. Environ Microbiol. 2001;3:502–11.

13. Stams AJM, Plugge CM. Electron transfer in syntrophic communities of anaerobic bacteria and archaea. Nat Rev Microbiol. 2009;7:568–77.
14. Glissmann K, Conrad R. Fermentation pattern of methanogenic degradation of rice straw in anoxic paddy soil. FEMS Microbiol Ecol. 2000;31:117–26.
15. Rui J, Peng J, Lu Y. Succession of bacterial populations during plant residue decomposition in rice field soil. Appl Environ Microbiol. 2009;75:4879–86.
16. Noll M, Klose M, Conrad R. Effect of temperature change on the composition of the bacterial and archaeal community potentially involved in the turnover of acetate and propionate in methanogenic rice field soil. FEMS Microbiol Ecol. 2010;73:215–25.
17. Schink B. Energetics of syntrophic cooperation in methanogenic degradation. Microbiol Mol Biol Rev. 1997;61:262–80.
18. McInerney MJ, Sieber JR, Gunsalus RP. Syntrophy in anaerobic global carbon cycles. Curr Opin Biotechnol. 2009;20:623–32.
19. Krylova NI, Janssen PH, Conrad R. Turnover of propionate in methanogenic paddy soil. FEMS Microbiol Ecol. 1997;23:107–17.
20. Mueller N, Worm P, Schink B, Stams AJM, Plugge CM. Syntrophic butyrate and propionate oxidation processes: from genomes to reaction mechanisms. Environ Microbiol Rep. 2010;2:489–99.
21. Hidalgo-Ahumada CAP, Nobu MK, Narihiro T, Tamaki H, Liu W-T, Kamagata Y, et al. Novel energy conservation strategies and behaviour of *Pelotomaculum schinkii* driving syntrophic propionate catabolism. Environ Microbiol. 2018;20:4503–11.
22. Thauer RK. Biochemistry of methanogenesis: a tribute to Marjory Stephenson. Microbiology. 1998;144:2377–406.
23. Conrad R. The global methane cycle: recent advances in understanding the microbial processes involved. Environ Microbiol Rep. 2009;1:285–92.
24. Haefele SM, Nelson A, Hijmans RJ. Soil quality and constraints in global rice production. Geoderma. 2014;235:250–9.
25. Deng N, Grassini P, Yang H, Huang J, Cassman KG, Peng S. Closing yield gaps for rice self-sufficiency in China. Nat Commun. 2019;10:1725.
26. Jiao S, Xu Y, Zhang J, Hao X, Lu Y. Core microbiota in agricultural soils and their potential associations with nutrient cycling. mSystems. 2019;4:e00313-18.
27. Zhang J, Lu Y. Conductive Fe3O4 nanoparticles accelerate syntrophic methane production from butyrate oxidation in two different lake sediments. Front Microbiol. 2016;7:1316.
28. Krumbock M, Conrad R. Metabolism of position-labeled glucose in anoxic methanogenic paddy soil and lake sediment. FEMS Microbiol Ecol. 1991;85:247–56.
29. Fadrosh DW, Ma B, Gajer P, Sengamalay N, Ott S, Brotman RM, et al. An improved dual-indexing approach for multiplexed 16S rRNA gene sequencing on the Illumina MiSeq platform. Microbiome. 2014;2:6.

30. Jeon Y-S, Park S-C, Lim J, Chun J, Kim B-S. Improved pipeline for reducing erroneous identification by 16S rRNA sequences using the Illumina MiSeq platform. J Microbiol. 2015;53:60–9.
31. Burke CM, Darling AE. A method for high precision sequencing of near full-length 16S rRNA genes on an Illumina MiSEq. PeerJ. 2016;4:2492.
32. Edgar RC, Haas BJ, Clemente JC, Quince C, Knight R. UCHIME improves sensitivity and speed of chimera detection. Bioinformatics. 2011;27:2194–200.
33. Parente E, Cocolin L, De Filippis F, Zotta T, Ferrocino I, O'Sullivan O, et al. FoodMicrobionet: a database for the visualisation and exploration of food bacterial communities based on network analysis. Int J Food Microbiol. 2016;219:28–37.
34. Capella-Gutierrez S, Silla-Martinez JM, Gabaldon T. trimAl: a tool for automated alignment trimming in large-scale phylogenetic analyses. Bioinformatics. 2009;25:1972–3.
35. Pruesse E, Peplies J, Gloeckner FO. SINA: accurate high-throughput multiple sequence alignment of ribosomal RNA genes. Bioinformatics. 2012;28:1823–9.
36. Asa E, Saafi M, Membah J, Billa A. Comparison of linear and nonlinear kriging methods for characterization and interpolation of soil data. J Comput Civ Eng. 2012;26:11–8.
37. Kursa MB, Rudnicki WR. Feature selection with the Boruta package. J Stat Softw. 2010;36:1–13.
38. Wickham H. ggplot2: elegant graphics for data analysis. New York: Springer; 2016.
39. Pesenti C, Navone SE, Guarnaccia L, Terrasi A, Costanza J, Silipigni R, et al. The genetic landscape of human glioblastoma and matched primary cancer stem cells reveals intratumour similarity and intertumour heterogeneity. Stem Cells Int. 2019. doi:10.1155/2019/2617030.
40. Hiemstra PH, Pebesma EJ, Twenhofel CJW, Heuvelink GBM. Real-time automatic interpolation of ambient gamma dose rates from the Dutch radioactivity monitoring network. Comput Geosci. 2009;35:1711–21.
41. Dailey AL. Metabolomic bioinformatic analysis. Methods Mol Biol. 2017;1606:341–52.
42. Yuen SC, Zhu H, Leung S-W. Building molecular interaction networks from microarray data for drug target screening. Methods Mol Biol. 2018;1762:179–97.
43. Zhang CY, Liu XL, Dong XZ. *Syntrophomonas curvata sp nov.*, an anaerobe that degrades fatty acids in co-culture with methanogens. Int J Syst Evol Microbiol. 2004;54:969–73.
44. Xia X, Zhang J, Song T, Lu Y. Stimulation of *Smithella*-dominating propionate oxidation in a sediment enrichment by magnetite and carbon nanotubes. Environ Microbiol Rep. 2019;11:236–48.
45. Qi W, Liu S, Zhao M, Liu Z. China's different spatial patterns of population growth based on the "Hu Line". J Geograph Sci. 2016;26:1611–25.
46. Zhou J, Deng Y, Shen L, Wen C, Yan Q, Ning D, et al. Temperature mediates continental-scale diversity of microbes in forest soils. Nat Commun. 2016;7:12083.
47. Guo X, Feng J, Shi Z, Zhou X, Yuan M, Tao X, et al. Climate warming leads to divergent succession of grassland microbial communities. Nat Clim Change. 2018;8:813–8.

48. Guo X, Zhou X, Hale L, Yuan M, Ning D, Feng J, et al. Climate warming accelerates temporal scaling of grassland soil microbial biodiversity. Nat Ecol Evol. 2019;3:612–9.
49. Hanselmann KW. Microbial energetics applied to waste repositories. Experientia. 1991;47:645–87.
50. Harmsen HJM, Van Kuijk BLM, Plugge CM, Akkermans ADL, De Vos WM, Stams AJM. *Syntrophobacter fumaroxidans sp. nov.*, a syntrophic propionate-degrading sulfate-reducing bacterium. Int J Syst Bacteriol. 1998;48:1383–7.
51. Imachi H, Sekiguchi Y, Kamagata Y, Hanada S, Ohashi A, Harada H. *Pelotomaculum thermopropionicum gen. nov., sp nov.*, an anaerobic, thermophilic, syntrophic propionate-oxidizing bacterium. Int J Syst Evol Microbiol. 2002;52:1729–35.
52. Sedano-Nunez VT, Boeren S, Stams AJM, Plugger CM. Comparative proteome analysis of propionate degradation by *Syntrophobacter fumaroxidans* in pure culture and in coculture with methanogens. Environ Microbiol. 2018;20:1842–56.
53. VanKuijk BLM, Stams AJM. Sulfate reduction by a syntrophic propionate-oxidizing bacterium. Anton Leeuw Int J G. 1995;68:293–6.
54. Rebac S, Visser A, Gerbens S, VanLier JB, Stams AJM, Lettinga G. The effect of sulphate on propionate and butyrate degradation in a psychrophilic anaerobic expanded granular sludge bed (EGSB) reactor. Environ Technol. 1996;17:997–1005.
55. Worm P, Koehorst JJ, Visser M, Sedano-Nunez VT, Schaap PJ, Plugge CM, et al. A genomic view on syntrophic versus non-syntrophic lifestyle in anaerobic fatty acid degrading communities. BBA-Bioenergetics. 2014;1837:2004–16.
56. Li Y, Sun Y, Li L, Yuan Z. Acclimation of acid-tolerant methanogenic propionate-utilizing culture and microbial community dissecting. Bioresour Technol. 2018;250:117–23.
57. Liu YT, Balkwill DL, Aldrich HC, Drake GR, Boone DR. Characterization of the anaerobic propioate-degrading syntrophs *Smithella propionica gen. nov., sp. nov*. and *Syntrophobacter wolinii*. Int J Syst Bacteriol. 1999;49:545–56.
58. de Bok FAM, Stams AJM, Dijkema C, Boone DR. Pathway of propionate oxidation by a syntrophic culture of *Smithella propionica* and *Methanospirillum hungatei*. Appl Environ Microbiol. 2001;67:1800–4.
59. Dolfing J. Syntrophic propionate oxidation via butyrate: a novel window of opportunity under methanogenic conditions. Appl Environ Microbiol. 2013;79:4515–6.
60. Lipson DA. The complex relationship between microbial growth rate and yield and its implications for ecosystem processes. Front Microbiol. 2015;6:615.
61. Beardmore RE, Gudelj I, Lipson DA, Hurst LD. Metabolic trade-offs and the maintenance of the fittest and the flattest. Nature. 2011;472:342–6.
62. Seel W, Derichs J, Lipski A. Increased biomass production by mesophilic food-associated bacteria through lowering the growth temperature from 30 °C to 10 °C. Appl Environ Microbiol. 2016;82:3754–64.

63. Thauer RK, Kaster A-K, Seedorf H, Buckel W, Hedderich R. Methanogenic archaea: ecologically relevant differences in energy conservation. Nat Rev Microbiol. 2008;6:579–91.

Figures

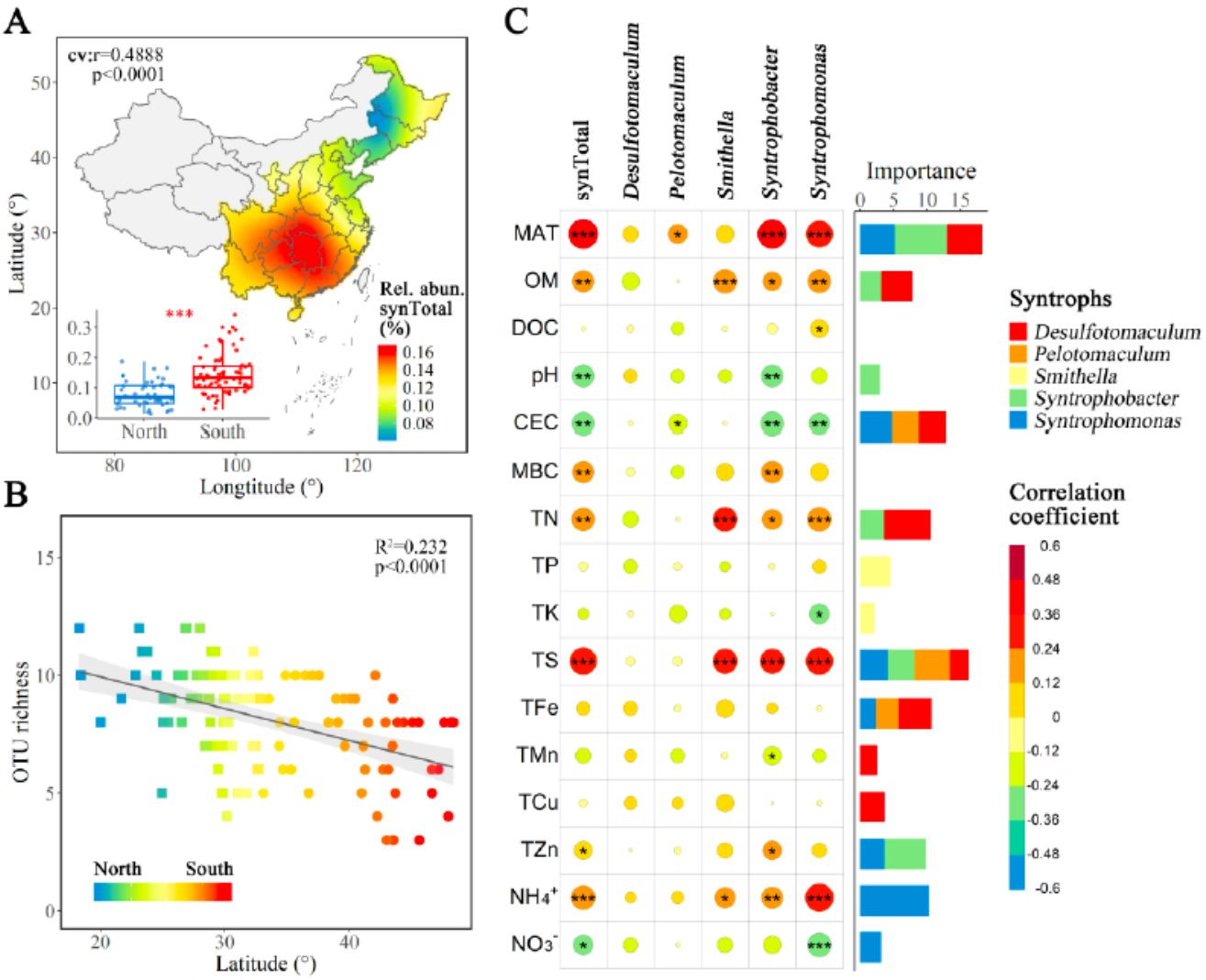

Figure 1

Biogeographic distribution of propionate syntrophs in paddy field soils across eastern China. (A) The map shows the spatial distribution of total relative abundance (Rel.abun.) of five syntroph genera (referred to synTotal) comprising Syntrophobacter, Pelotomaculum, Smithella, Desulfotomaculum and Syntrophomonas together. The map was build using Kriging interpolation method with cross-validation (cv) based on Pearson correlation. The inset in lower-left corner shows the difference in mean relative abundance of synTotal between the low (South) and the high (North) latitude soils. The red asterisks indicate the significant difference at $P \leq 0.001$. (B) The α-diversity of propionate syntrophs expressed as OTU richness, which decreases with the increase of latitude. The solid line denotes the least-squares

linear regression, which was significant at P < 0.0001. (C) Correlations between the relative abundance of propionate syntrophs (either in total or individually) and environmental factors. The color and size of circles indicate the Spearman correlation coefficients. The black asterisks indicate the significant correlations: * 0.01 < P ≤ 0.05, ** 0.001 P ≤ 0.01, *** P ≤ 0.001. Bars in the right show the importance of environmental factors to five syntroph genera estimated based on Boruta algorithm. The environmental factors include the mean annual temperature (MAT) and fifteen edaphic factors: the content of soil organic matter (OM), dissolved organic carbon (DOC), pH, cation exchange capacity (CEC), microbial biomass carbon (MBC), the total contents of N, P, K, S, Fe, Mn, Cu, Zn (TN, TP, TK, TS, TFe, TMn, TCu, TZn), ammonium (NH4+) and nitrate (NO3-).

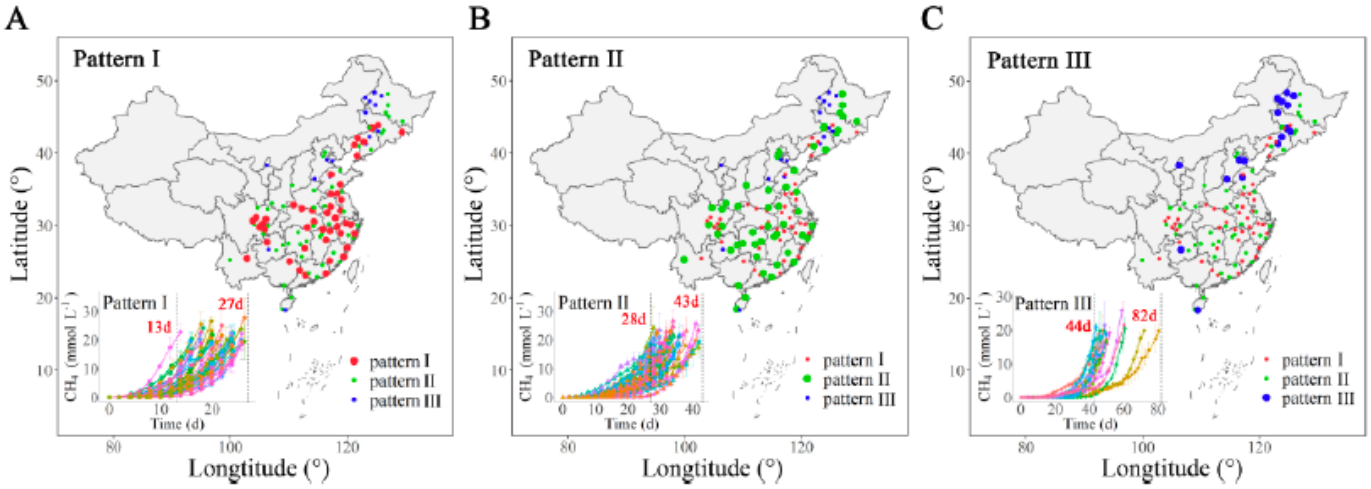

Figure 2

Geographic feature of propionate degradation in paddy field soils. The duration by which CH4 production reached to the quantity corresponding to >90% degradation of propionate added was defined as the time lapse. Three patterns can be distinguished from 113 paddy field soils analyzed. (A) Pattern I, representing the fast rate group, comprises 45 soil samples (red dots), having the time lapse of 13 d to 27 d. (B) Pattern II, representing the medium rate group, includes 51 soil samples (green dots), with the time lapse of 28 d to 43 d. (C) Pattern III, the slow rate group, contains 17 soil samples (blue dots), having the time lapse of 44 d to 82 d. The CH4 production curves of each soil in three groups are illustrated in the lower-left corner of each panel. The CH4 production curves within each group are colored randomly and two vertical grey dot lines denote the ranges of time lapse. The error bars indicate the standard deviation of three replicates. All soil samples are displayed in maps with the pattern-specific samples highlighted by the increased sizes of the colored dots (red for Pattern I, green for Pattern II and blue for Pattern III).

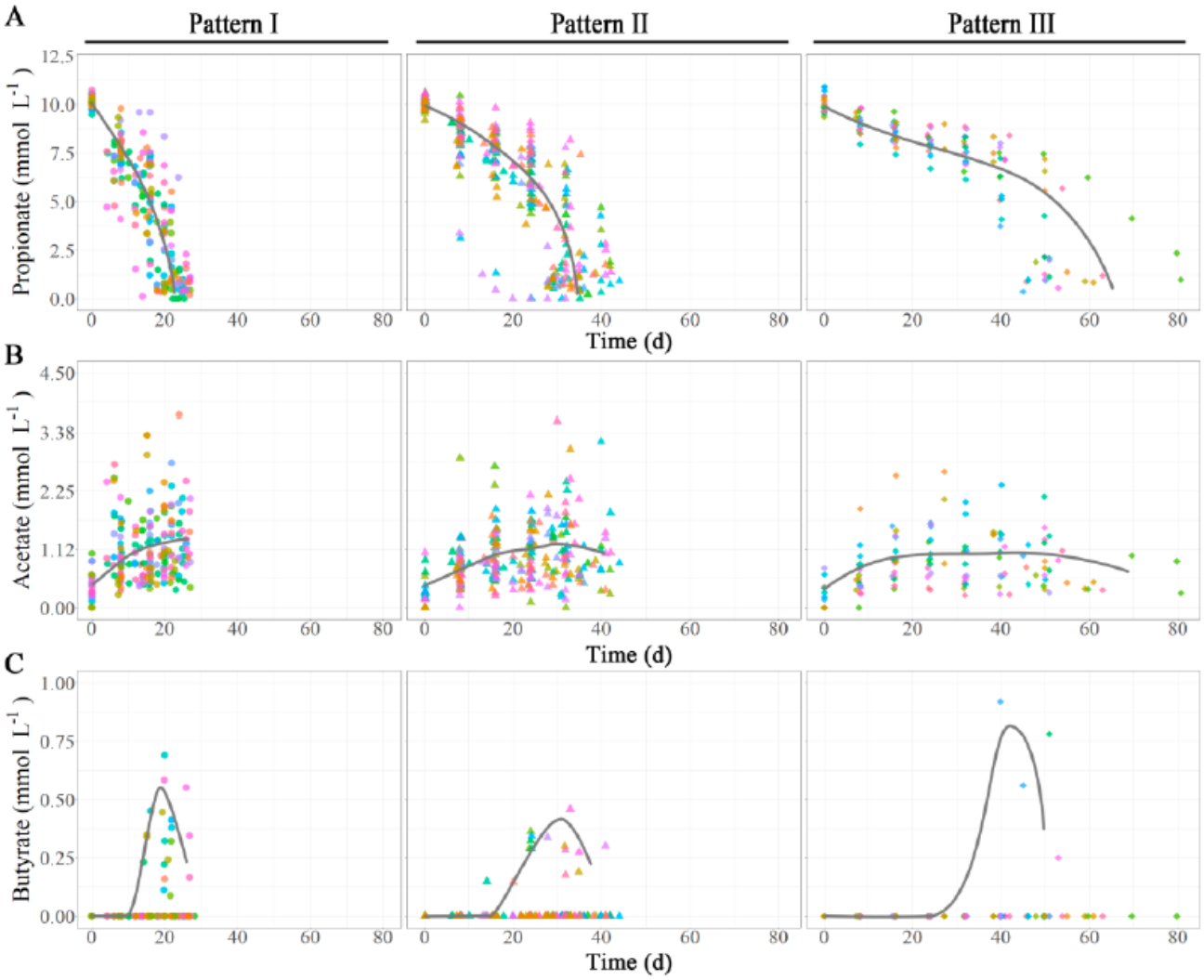

Figure 3

The dynamics of short-chain fatty acids in paddy soils over anaerobic incubation. Propionate was added at a concentration of 10 mM to each soil samples, which were incubated anaerobically until at least >90% of propionate oxidized. (A) The consumption of propionate. (B and C) The transient accumulations of acetate and butyrate, respectively. Soil samples are separated into three groups in accordance with three patterns revealed by methanogenesis, circles for Pattern I, triangles for Pattern II and diamonds for Pattern III. Soil samples within each group are colored randomly.

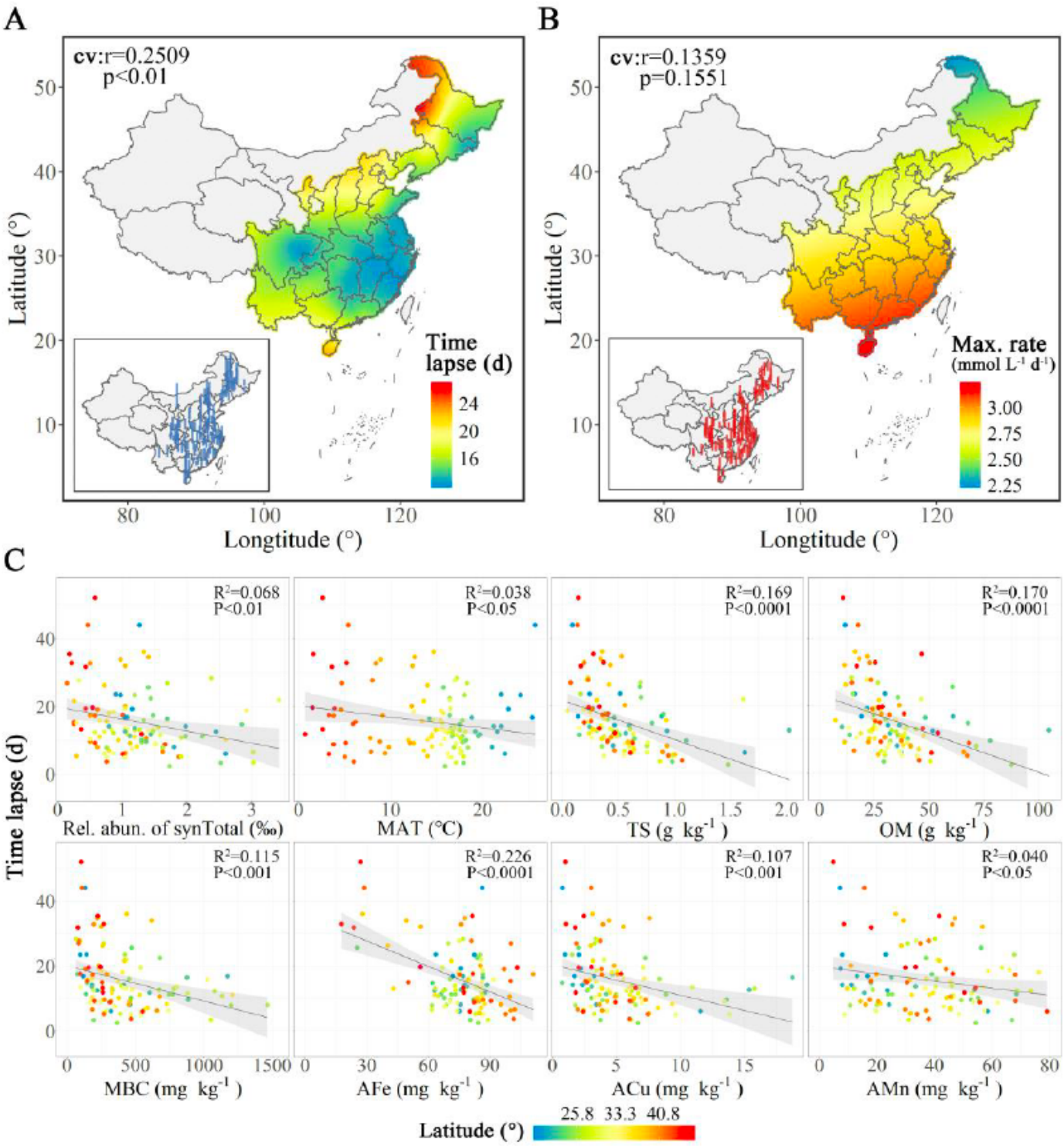

Figure 4

Geographical distribution of syntroph functioning potential and the correlative factors. (A) The map showing the functioning potential expressed as the time lapse for propionate degradation. The shorter the time lapse, the higher the functioning potential. (B) The map showing the functioning potential expressed as the maximum rate of CH4 production, which was estimated during the period when CH4 concentration was at the linear increase. The maps in (A) and (B) were build using Kriging interpolation

method. The insets in the lower-left corner of each panel display the actual values of the time lapse (blue) and the maximum rate (red) of CH4 production, respectively. (C) The correlations of the time lapse with the relative abundance of total syntrophs (Rel. abun. of synTotal), the mean annual temperature (MAT), the contents of total soil S (TS), organic matter (OM), microbial biomass carbon (MBC), and the bioavailable contents of Fe, Cu and Mn (AFe, ACu, AMn). The solid lines denote the least-squares linear regressions. Individual soil samples are colored from blue to red in correspondence with their locations from the low latitudes to the high latitudes.

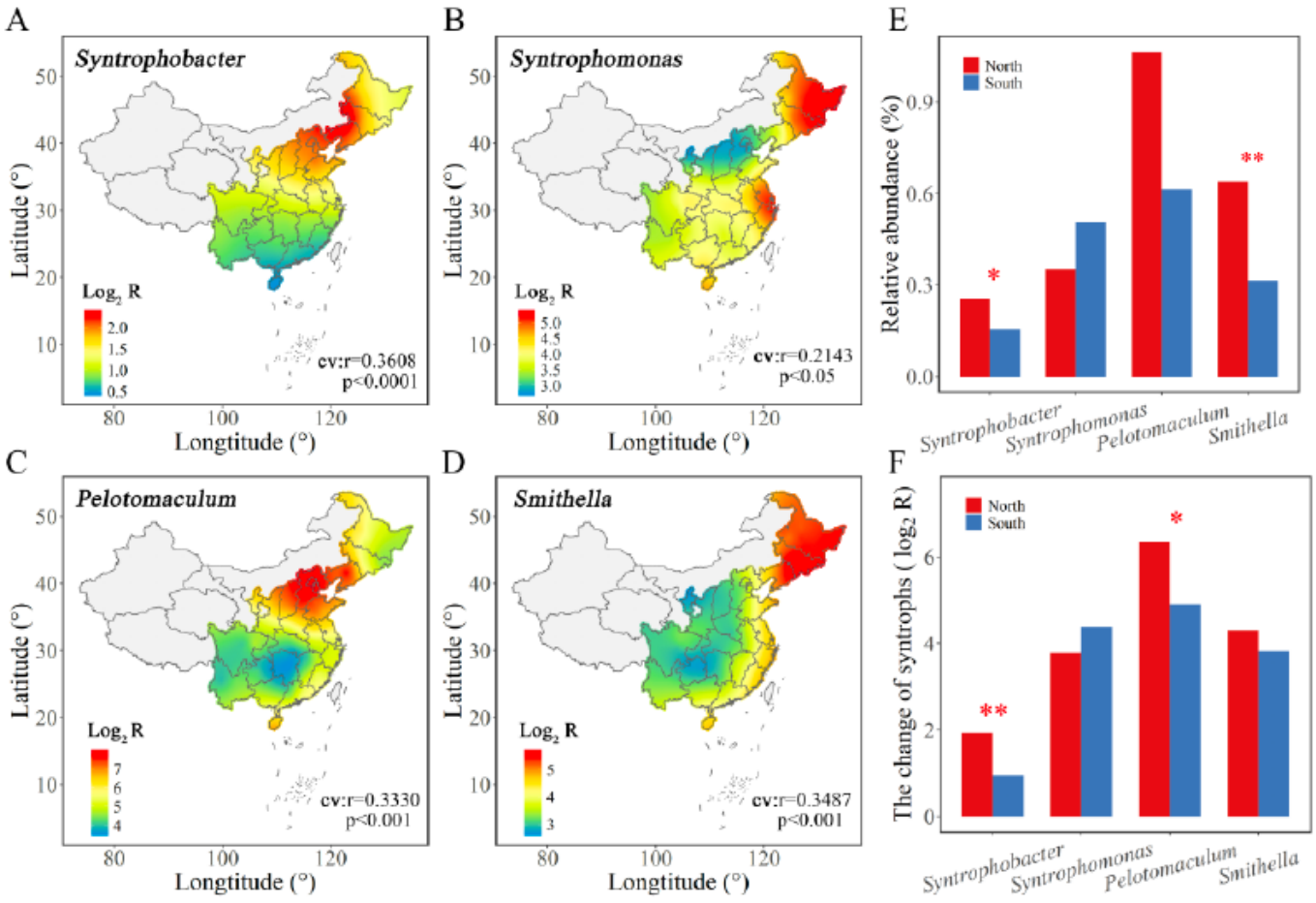

Figure 5

The relative growth of propionate syntrophs during anaerobic incubation. The relative growth was expressed as the logarithmic (log2) fold change (R) in relative abundance of individual syntroph genera over the anaerobic incubation. (A-D) The geographic distributions of relative growth of Syntrophobacter, Syntrophomonas, Pelotomaculum and Smithella, respectively. (E) The mean relative abundances of four syntroph genera at the end of anaerobic incubation. (F) The mean log2 fold change (R) in relative abundance of four syntroph genera. Soil samples in (E) and (F) were clustered into two geographic groups for the low latitude regions (South) and the high latitude regions (North), respectively. The red asterisks denote the significant differences between the “South” and “North” groups: * $0.01 < P \leq 0.05$, ** $P \leq 0.01$.

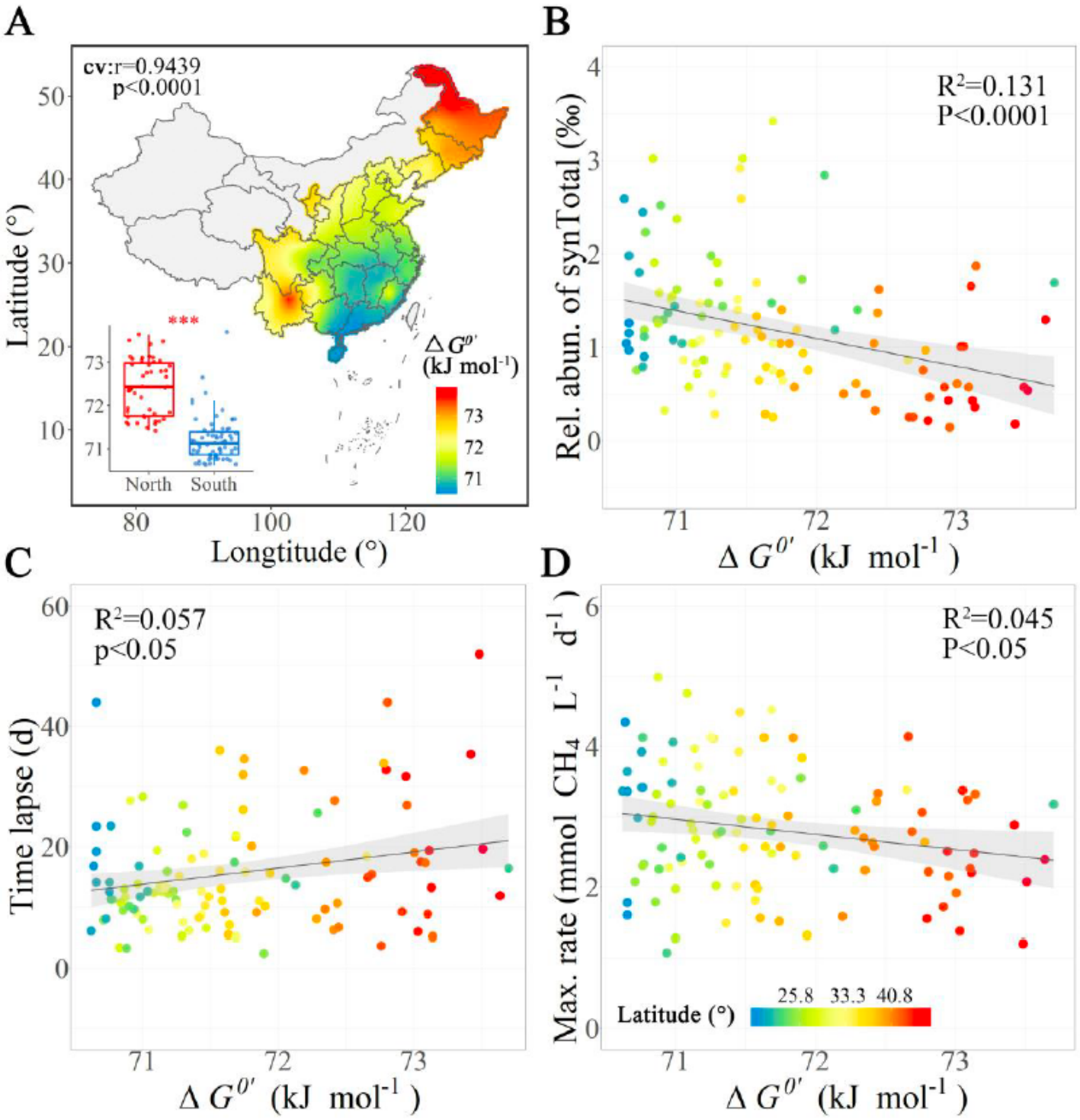

Figure 6

The geographical feature of standard Gibbs free energy change for propionate degradation. (A) The geographic distribution of standard Gibbs free energy change for propionate oxidation corrected by temperature (△G0'). The mean summer temperature (from June to September) at sampling sites was used to correct the calculation of standard Gibbs free energy change for the reaction: CH3CH2COO-(aq) + 2H2O(l) — CH3COO-(aq) + 3H2(g) + CO2(g). The values of standard Gibbs free energy change (△G0) and

enthalpy change (△H0) at 25°C (i.e. 298.15 K, 100 kPa, 1 M) equal to +71.6 kJ and +152.3 kJ per mol of propionate, respectively. The inset in lower-left corner shows the difference in mean △G0’ between two geographic groups for the low (South) and the high (North) latitude soils, respectively. The red asterisks indicate the significant difference at $P \leq 0.001$. (B) The correlation of synTotal relative abundance with △G0’. (C) The correlation of time lapse for propionate degradation with △G0’. (D) The correlation of maximum rate of CH_4 production with △G0’. The solid lines in (B-D) denote the least-squares linear regressions. Individual soil samples are colored from blue to red in correspondence with their locations from the low latitudes to the high latitudes.